IOP Publishing Plasma Sources Science and Technology
Plasma Sources Sci. Technol. **26** (2017) 024008 (14pp) https://doi.org/10.1088/1361-6595/aa56e2

Characteristics and transport effects of the electron drift instability in Hall-effect thrusters

T Lafleur[1,2], S D Baalrud[3] and P Chabert[1]

[1] Laboratoire de Physique des Plasmas, CNRS, Sorbonne Universités, UPMC Univ Paris 06, Univ Paris-Sud, Ecole Polytechnique, F-91128 Palaiseau, France
[2] Centre National d'Etudes Spatiales (CNES), F-31401 Toulouse, France
[3] Department of Physics and Astronomy, University of Iowa, Iowa City, IA 52242, United States of America

E-mail: trevor.lafleur@lpp.polytechnique.fr

Received 29 July 2016, revised 16 November 2016
Accepted for publication 4 January 2017
Published 31 January 2017

Abstract

The large electron $\mathbf{E} \times \mathbf{B}$ drift (relative to the ions) in the azimuthal direction of Hall-effect thrusters is well known to excite a strong instability. In a recent paper (Lafleur *et al* 2016 *Phys. Plasmas* **23** 053503) we demonstrated that this instability leads to an enhanced electron–ion friction force that increases the electron cross-field mobility to levels similar to those seen experimentally. Here we extend this work by considering in detail the onset criteria for the formation of this instability (both in xenon, and other propellants of interest), and identify a number of important characteristics that it displays within Hall-effect thrusters (HETs): including the appearance of an additional non-dimensionalized scaling parameter (the instability growth-to-convection ratio), which controls the instability evolution and amplitude. We also investigate the effect that the instability has on electron and ion heating in HETs, and show that it leads to an ion rotation in the azimuthal direction that is in agreement with that seen experimentally.

Keywords: Hall-effect thruster, electron drift instability, anomalous electron transport, alternative propellants

(Some figures may appear in colour only in the online journal)

1. Introduction

Hall-effect thrusters (HETs) are one of the most important plasma technologies used to provide propulsion for a range of different industrial and research space missions [1]. HETs are complex devices that display a surprising richness of physical phenomena [2, 3], as evidenced by the many different oscillations and instabilities present during typical operation. These oscillations span a wide frequency range and include for example, low frequency (10s of kHz) breathing-mode [1, 4] and rotating-spoke oscillations [5, 6], medium frequency (100s of kHz) transit-time oscillations [7], and high-frequency (1–10 MHz) streaming [8] and electron drift instabilities [9, 10] (see [11] for a more detailed list of known HET oscillations).

Of the many oscillations, the electron drift instability (EDI) has attracted interest for its possible role in enhancing electron transport across the radial magnetic field [9, 12]. The EDI is viewed as a kinetic instability that forms due to the large electron drift velocity (relative to the ions) in the azimuthal $\mathbf{E} \times \mathbf{B}$ direction, and represents a coupling between electron Bernstein modes and ion acoustic waves. This instability has been observed experimentally [13] and in 1D [14, 15], 2D [9, 16, 17], and 3D [18, 19] particle-in-cell (PIC) simulations. In contrast to other azimuthal instabilities such as fluid gradient-drift modes [20] (10's of kHz to MHz), or the more commonly known rotating-spoke modes associated with neutral depletion [5, 21] (10's of kHz), which have large wavelengths (cm's), the EDI is a short wavelength (mm's), high-frequency (MHz) kinetic drift instability. Recently [12] it has been shown that the EDI gives rise to an enhanced

electron–ion friction force that can increase the electron cross-field mobility by 1–3 orders of magnitude (compared with classical electron–neutral or electron–ion Coulomb collisions): in agreement with experimental results.

The EDI has previously been studied theoretically within a HET context [10, 22] where the relevant dispersion relation has been derived and the effect of non-Maxwellian electron distribution functions and plasma density gradients investigated. As a result of the applied magnetic field, the dispersion relation is quantized and shows narrow wavenumber bands within which the growth rate is positive. However, when considering the wavenumbers that can be accommodated by the finite HET radial channel width, this discrete spectrum tends to be replaced by a continuous spectrum (as verified experimentally [13, 23]) similar to that for ion acoustic waves. This modified ion acoustic type dispersion relation has not been studied in detail though, and a number of questions remain unclear. For example, what are the physical criteria leading to an unstable dispersion relation and hence the formation of the instability? Can the instability be damped by collisions with the residual neutral gas inside and in the near-plume region of the thruster? What is the role of the ion mass on the instability, and can different masses influence the instability threshold? This last point is of particular importance because most HET research has been performed using xenon, and there is renewed interest in finding alternative propellants [24–26] that are cheaper and more easily available. Finally, experiments show the presence of periodic erosion patterns [27, 28] on the ceramic walls of HET channels with wavelengths similar to those for the EDI ($\sim$1 mm). Thus it is natural to ask whether the EDI is responsible for the appearance of these patterns.

There also remains a worrying apparent discrepancy when considering the EDI as the cause of the enhanced electron cross-field transport. All previous fluid or hybrid HET simulations require an anomalously high electron mobility in order to get physically meaningful results and agreement with experiment, and this is usually achieved by artificially increasing the electron collisionality [4, 29–36]. But if this increased collisionality results from the EDI, then one would expect that an additional electron heating term (accounting for the power deposition by the azimuthal electrostatic wave) would also be needed. Furthermore, if the EDI is strong enough to significantly affect the electron transport, does it have any effect on the ion transport?

In this paper we specifically aim to address the above issues by considering in detail the modified dispersion relation for the EDI, as well as the global effects this instability has on the charged particle transport in HETs.

2. Instability characteristics

2.1. Dispersion relation

In [12] we derived the complete dispersion relation of the EDI for mutually perpendicular electric and magnetic fields assuming drifting Maxwellian distributions for the electrons and ions. To simplify the analysis this was performed using a Cartesian coordinate system where the 'axial' thruster direction is along the z-axis, the 'radial' direction is along the x-axis, and the 'azimuthal' $\mathbf{E} \times \mathbf{B}$ direction is along the y-axis. The resulting dispersion relation agrees with that independently obtained in [10] (aside from the ion drift that we have included) and is given by

$$0 = 1 - \frac{\omega_{pi}^2}{k^2 v_{Ti}^2} Z'\left(\frac{\omega - \mathbf{k}\cdot\mathbf{v}_{di}}{k v_{Ti}}\right) + \frac{1}{k^2 \lambda_{\mathrm{De}}^2}\left[1 + \left(\frac{\omega - k_y v_{ye}}{k v_{Te}}\right) \times \sum_{n=-\infty}^{\infty} \mathrm{e}^{-\beta} I_n(\beta) Z\left(\frac{\omega - k_y v_{ye} - n\omega_{ce}}{k_x v_{Te}}\right)\right], \quad (1)$$

where $\omega_{pi} = \sqrt{\frac{q^2 n_i}{\epsilon_0 M}}$ is the ion plasma frequency, $|q|$ is the elementary charge, n_i is the ion density, ϵ_0 is the permittivity of free space, M is the ion mass, $v_{Ti} = \sqrt{\frac{2\,|\,q\,|\,T_i}{M}}$ is the ion thermal velocity, T_i is the ion temperature (in eV), $k = \sqrt{k_x^2 + k_y^2 + k_z^2}$ is the magnitude of the wavevector $\mathbf{k}$ with k_x, k_y, and k_z mutually orthogonal components, ω is the wave frequency, Z is the plasma dispersion function [37], $\lambda_{\mathrm{De}} = \sqrt{\frac{\epsilon_0 T_e}{|\,q\,|\,n_e}}$ is the electron Debye length, T_e is the electron temperature (in eV), n_e is the electron density, $v_{ye} = \frac{E_z}{B_x}$ is the 'azimuthal' electron drift velocity with E_z and B_x the 'axial' and 'radial' magnetic field components, $v_{Te} = \sqrt{\frac{2\,|\,q\,|\,T_e}{m}}$ is the electron thermal velocity, m is the electron mass, $\beta = \frac{k_\perp^2 v_{Te}^2}{2\omega_{ce}}$, $k_\perp = \sqrt{k_y^2 + k_z^2}$, $\omega_{ce} = \frac{|\,q\,|\,B_x}{m}$ is the electron cyclotron frequency, and I_n are modified Bessel functions of the first kind. Depending on the plasma parameters, equation (1) can exhibit discrete, sharply-peaked, frequency and growth rate bands as a function of wavenumber (see for example [10, 12, 22]).

Because the azimuthal direction of a HET is closed, only discrete values of the azimuthal wavenumber (k_y in the coordinate system used here) can meet this closed boundary condition. However, since the wavenumbers of interest satisfy, $\frac{1}{k_y} \sim \lambda_{\mathrm{De}} \ll 2\pi R$ (where R is a characteristic radius of the thruster), the azimuthal spectrum is essentially continuous. Similarly, the radial wavenumber (k_x here) is also discrete because of the finite width of the radial HET walls. As a result, the minimum value that the radial wavenumber can take is, $k_x \sim \frac{1}{\Delta R}$ (where ΔR is the radial width of the channel). For $k_x > \frac{1}{\Delta R}$ it has been shown previously [12, 22] that the sharply-peaked frequency and growth rate bands in equation (1) tend to disappear, and that equation (1) simplifies to a modified ion acoustic type dispersion relation

$$0 = 1 - \frac{\omega_{pi}^2}{k^2 v_{Ti}^2} Z'\left(\frac{\omega + \mathrm{i}\nu_{in} - \mathbf{k}\cdot\mathbf{v}_{di}}{k v_{Ti}}\right) - \frac{\omega_{pe}^2}{k^2 v_{Te}^2} Z'\left(\frac{\omega + \mathrm{i}\nu_{en} - \mathbf{k}\cdot\mathbf{v}_{de}}{k v_{Te}}\right). \quad (2)$$

Here we have now also accounted for the effects of ion–neutral, ν_{in}, and electron–neutral, ν_{en}, collisions using a constant collision frequency model given by $\left(\frac{\partial f_s}{\partial t}\right)_c = \nu_{sn} f_s$ for each species (where f_s is the total distribution function), as well as allowed for an electron drift in all directions. Note that in this form of the dispersion relation the only role of the magnetic field is to provide an azimuthal electron drift velocity. Although we will treat the complete expression in equation (2) when investigating criteria for instability onset, it is useful to obtain an approximate dispersion relation to elucidate certain important characteristics. To do this we perform a large argument expansion ($\zeta \gg 1$) of the plasma dispersion function [37] for the ions, $Z'(\zeta) \approx \frac{1}{\zeta^2} - 2\mathrm{i}\sqrt{\pi}\zeta \mathrm{e}^{-\zeta^2}$, and a small argument expansion ($\zeta \ll 1$) for the electrons, $Z'(\zeta) \approx -2 - 2\mathrm{i}\sqrt{\pi}\zeta \mathrm{e}^{-\zeta^2} \approx -2 - 2\mathrm{i}\sqrt{\pi}\zeta$. Thus equation (2) becomes

$$0 = 1 + \frac{1}{k^2\lambda_{\mathrm{De}}^2} - \frac{\omega_{pi}^2}{(\omega + \mathrm{i}\nu_{in} - \mathbf{k}\cdot\mathbf{v}_{di})^2} + \mathrm{i}\frac{\sqrt{\pi}}{k^2\lambda_{\mathrm{De}}^2}\left\{\frac{\omega + \mathrm{i}\nu_{en} - \mathbf{k}\cdot\mathbf{v}_{de}}{kv_{Te}} + \frac{T_e}{T_\mathrm{i}}\left(\frac{\omega + \mathrm{i}\nu_{in} - \mathbf{k}\cdot\mathbf{v}_{di}}{kv_{Ti}}\right) \times \exp\left[-\frac{(\omega + \mathrm{i}\nu_{in} - \mathbf{k}\cdot\mathbf{v}_{di})^2}{k^2 v_{Ti}^2}\right]\right\}. \quad (3)$$

Setting $\omega = \omega_R + \mathrm{i}\gamma$ and solving, we obtain an approximate dispersion relation for the EDI

$$\omega_R \approx \mathbf{k}\cdot\mathbf{v}_{di} \pm \frac{kc_s}{\sqrt{1 + k^2\lambda_{\mathrm{De}}^2}}, \quad (4)$$

$$\gamma \approx -\nu_{in} - \sqrt{\frac{\pi}{8}}\frac{kc_s}{(1 + k^2\lambda_{\mathrm{De}}^2)^2}\left\{\left(\frac{T_e}{T_i}\right)^{3/2} \times \exp\left(-\frac{T_e}{2T_i}\frac{1}{1 + k^2\lambda_{\mathrm{De}}^2}\right) + \sqrt{\frac{m}{M}}\left[1 \mp \frac{\mathbf{k}\cdot(\mathbf{v}_{di} - \mathbf{v}_{de})}{kc_s}\sqrt{1 + k^2\lambda_{\mathrm{De}}^2}\right]\right\}, \quad (5)$$

where $c_s = \sqrt{\frac{|q|T_e}{M}}$ is the ion sound speed. By observing equation (5) we see that both ion–neutral collisions, and a term consisting of the electron–ion temperature ratio (which effectively represents ion Landau damping), act to damp the instability. In this first order approximation it is also seen that electron–neutral collisions do not contribute to the damping. Since the azimuthal electron drift velocity is very high in HETs, any instability is expected to have $\mathbf{k} \approx k_y\hat{\mathbf{j}}$, and thus equation (5) can be further simplified in the limit that, $\frac{T_e}{T_i} \gg 1$, $\frac{\mathbf{k}\cdot(\mathbf{v}_{di} - \mathbf{v}_{de})}{c_s} \gg 1$ and $\nu_{in} \to 0$ to give

$$\gamma \approx \pm\sqrt{\frac{\pi m}{8M}}\frac{k_y v_{ye}}{(1 + k_y^2\lambda_{\mathrm{De}}^2)^{3/2}}. \quad (6)$$

The wavenumber giving maximum growth, $k_{\max}$, can easily be found from, $\frac{\mathrm{d}\gamma}{\mathrm{d}k_y} = 0$, which yields

$$k_{\max} = \frac{1}{\sqrt{2}\,\lambda_{\mathrm{De}}}. \quad (7)$$

From this wavenumber we can then obtain simple approximate formulas for the wave frequency, maximum growth rate, and instability phase velocity

$$\omega_R \approx \frac{\omega_{pi}}{\sqrt{3}}, \quad (8)$$

$$\gamma_{\max} \approx \sqrt{\frac{\pi m}{54M}}\frac{v_{ye}}{\lambda_{\mathrm{De}}}, \quad (9)$$

$$v_{\mathrm{phase}} = \frac{\omega_R}{k_y} \approx \sqrt{\frac{2}{3}}\,c_s. \quad (10)$$

For typical plasma densities ($\sim 10^{17}$ m^{-3}) and electron temperatures ($\sim$20 eV), the instability wavelength, frequency, and phase velocity are about 1 mm, 3.5 MHz, and 3000 m s^{-1}, respectively.

2.2. Instability modes

From equations (4) and (5) we see that there are two modes, ω_R^+, γ^+, and ω_R^-, γ^-. If we pick a wavevector, $\mathbf{k}_1$, which gives $\gamma^+ > 0$, then we see that automatically the wavevector, $-\mathbf{k}_1$, will give $\gamma^- > 0$ and $\gamma^- = \gamma^+$. Consider now the group velocity of the instability

$$\mathbf{v}_g = \frac{\partial\omega_R}{\partial\mathbf{k}} = \mathbf{v}_{di} \pm \frac{\mathbf{k}}{k}\frac{c_s}{(1 + k^2\lambda_{\mathrm{De}}^2)^{3/2}}. \quad (11)$$

Using the wavevectors $\mathbf{k}_1$ and $-\mathbf{k}_1$ again, we can easily see that

$$\mathbf{v}_g^+ = \mathbf{v}_{di} + \frac{\mathbf{k}_1}{k_1}\frac{c_s}{(1 + k_1^2\lambda_{\mathrm{De}}^2)^{3/2}}, \quad (12)$$

$$\mathbf{v}_g^- = \mathbf{v}_{di} - \frac{(-\mathbf{k}_1)}{k_1}\frac{c_s}{(1 + k_1^2\lambda_{\mathrm{De}}^2)^{3/2}} = \mathbf{v}_{di} + \frac{\mathbf{k}_1}{k_1}\frac{c_s}{(1 + k_1^2\lambda_{\mathrm{De}}^2)^{3/2}}. \quad (13)$$

Similarly, the instability phase velocity in the azimuthal direction, $v_{\mathrm{phase}} = \frac{\omega_R}{k_y}$, is also equal for both modes. We therefore conclude that both modes are in fact the same, and hence that only a single unstable mode is present.

2.3. Instability thresholds

In deriving equation (2) (and subsequent approximations) we have used a Maxwellian distribution function. In our previous work [12] we showed that the EDI can grow very rapidly and enter a nonlinear regime before eventually saturating. In this regime the electron distribution is almost certainly non-Maxwellian, and we implicitly accounted for this by considering a generalized dispersion relation coupled to a conservation equation for the instability energy density. This method however does not allow the complete distribution function to be explicitly determined. In the present section we are not interested in this nonlinear regime, but rather in what conditions *lead* to instability, for which it is sufficient to

consider a Maxwellian distribution. If ion–neutral collisions are negligible, then from equation (5) the growth rate for the instability is positive only if

$$\frac{kc_s}{\sqrt{1+k^2\lambda_{\mathrm{De}}^2}}\left[1+\sqrt{\frac{M}{m}}\left(\frac{T_e}{T_i}\right)^{3/2}\exp\left(-\frac{T_e}{2T_i}\frac{1}{1+k^2\lambda_{\mathrm{De}}^2}\right)\right] < |\mathbf{k}\cdot(\mathbf{v}_{di}-\mathbf{v}_{de})|. \tag{14}$$

This equation shows clearly that the driving force for the instability is the flow difference, $\Delta\mathbf{v}=\mathbf{v}_{di}-\mathbf{v}_{de}$, between the ions and electrons. In the radial direction there is not expected to be any significant flow difference (except perhaps in the thin sheath regions), but we note that flow differences do exist in both the axial and azimuthal directions. In the axial direction ions are moving downstream whereas electrons are moving upstream towards the anode, thus the flow difference is effectively increased. Because of the radial magnetic field, the electron mobility is strongly reduced, but in certain regions of the discharge the electron axial velocity can be of a similar magnitude to the ion axial velocity. In the azimuthal direction the ion velocity (if any) is very small, but because the electrons are magnetized, they experience an $\mathbf{E}\times\mathbf{B}$ drift approximately given by, $v_{ye}=\frac{E_z}{B_x}$. For typical electric (2×10^4 V m^{-1}) and magnetic (200 G) fields, this gives a large drift velocity of about 1×10^6 m s^{-1}, which is of the order of the electron thermal velocity itself. Thus the EDI is driven primarily by the electron–ion flow difference in the azimuthal direction.

Although the unstable nature of the EDI has been discussed before in a number of previous works [10, 22, 55, 58], threshold conditions for the onset of such an instability have not been explicitly studied. Our aim here is to investigate this onset, and to provide a simple graphical reference that can be used to estimate whether the EDI is expected to be present for a given set of conditions, and which wavenumbers are unstable. Although equation (14) provides a convenient expression for the threshold conditions of equation (2) in the limit $\frac{T_e}{T_i}\gg1$, exact instability thresholds for the collisionless limit ($\nu_{sn}=0$) can be computed directly from equation (2) using the Penrose criterion [38]. This states that a necessary and sufficient condition for instability is provided by

$$P(F)=\int_{-\infty}^{\infty}\mathrm{d}u\frac{F(u)-F(u_0)}{(u-u_0)^2}>0, \tag{15}$$

where

$$F(u)=\sum_s\frac{q_s^2}{\epsilon_0 m_s}\int\mathrm{d}^3v f_{s0}(\mathbf{v})\delta(u-\hat{\mathbf{k}}\cdot\mathbf{v}) \tag{16}$$

is a projection of the distribution function along the wavevector. Here f_{s0} is the equilibrium component of the distribution function, and u_0 is the location of the central minimum of $F(u)$, which is located between the two peaks of $F(u)$: $u_1<u_0<u_2$. Figure 1 shows the instability diagram for a xenon plasma as a function of the temperature ratio, $\frac{T_e}{T_i}$, and normalized flow speed difference, $\frac{\Delta v}{c_s}$. Here we have

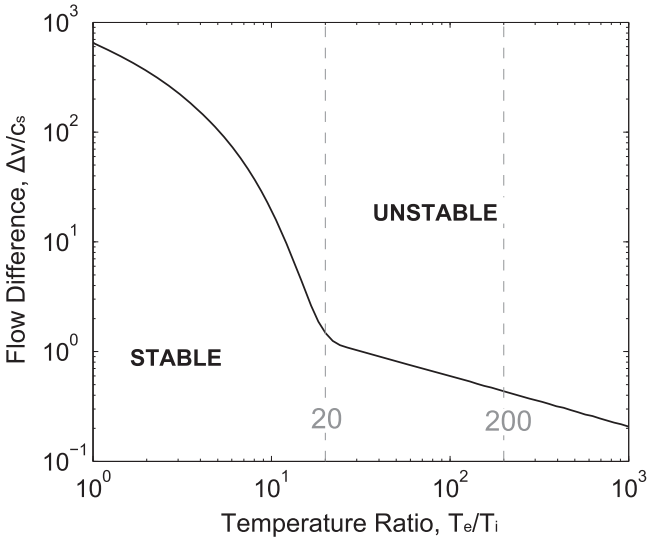

Figure 1. Stability diagram for Xe^+ as a function of the electron–ion flow speed difference, $\frac{\Delta v}{c_s}$, and electron–ion temperature ratio, $\frac{T_e}{T_i}$. Parameters above the curve lead to an unstable plasma. The vertical dashed lines mark temperature ratios of 20 and 100 respectively.

assumed that the instability is predominantly in the azimuthal direction so that $\mathbf{k}\approx k_y\hat{\mathbf{j}}$. Since, $c_s\sim5000$ m s^{-1}, in typical HETs we have, $\frac{\Delta v}{c_s}\sim100$. From figure 1 we see that this falls in the unstable region of the diagram, indicating that the EDI will develop. In fact, since $\Delta v>c_s$ in most of the HET channel, and for typical electron–ion temperature ratios (see the dashed lines in figure 1), instability is predicted essentially throughout the thruster and near-plume region (i.e. not just at the maximum electric field location).

The Penrose criterion can also be used to determine the range of unstable wavenumbers, $k_{\mathrm{min}}^2<k^2<k_{\mathrm{max}}^2$. Here, $k_{\mathrm{max}}^2=P(F)$ is calculated from equation (15), and $k_{\mathrm{min}}=\max\{0,\bar{k}\}$, where [39]

$$\bar{k}^2\equiv\int_{-\infty}^{\infty}\mathrm{d}u\frac{F(u)-F(u_2)}{(u-u_2)^2}. \tag{17}$$

Figure 2 shows contours for the threshold wavenumber at several values of the electron–ion flow speed difference. As expected, the range of unstable wavenumbers broadens as the flow speed difference increases. We also see that instability occurs for wavenumbers of the order of $k\lambda_{\mathrm{De}}\sim1$ (giving wavelengths of the mm level).

The Penrose criterion only applies to collisionless plasmas and so cannot be used to study the effects of ion–neutral collisions. Therefore we instead make use of the approximate dispersion relation from equations (4) and (5) to investigate collisional effects on the EDI instability thresholds. Figure 3 shows the pressure thresholds for a xenon plasma, and indicates which values of $\frac{\Delta v}{c_s}$ are needed in order to obtain instability for a given pressure. The vertical dashed lines show the typical pressures near the thruster exit and anode regions of HETs (for a mass flow rate of about 5 kg s^{-1} and an inner and outer channel radius of 2 cm and 4 cm, respectively). Within this pressure range we see that as the plasma density

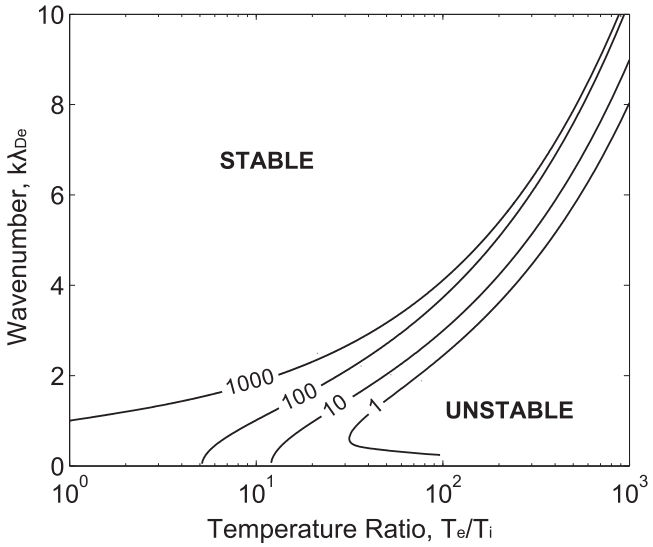

Figure 2. Wavenumbers leading to instability as a function of the electron–ion temperature ratio, $\frac{T_e}{T_i}$. The curves correspond to different electron–ion flow speed differences, $\frac{\Delta v}{c_s}$. Parameters below the curves lead to an unstable plasma.

increases (contours in figure 3) the flow difference needed is reduced, while as the electron–ion temperature ratio decreases, the required flow difference increases. Nevertheless, since $\frac{\Delta v}{c_s} \sim 100$, we see that instability is again predicted essentially throughout the thruster. This indicates that ion–neutral collisions are too weak to damp the instability.

2.4. Alternative propellants

Because of the cost and scarcity of xenon, there is interest in investigating alternative propellants for HETs. Testing with such alternative propellants has typically involved other noble gases such as krypton [24], although more recently iodine has been identified as a promising candidate because of its lower cost, higher availability, and its ability to be stored as a solid [25, 26]. The influence of the propellant (and hence ion mass) on electron transport has however not seen any significant research, and it is not clear if the EDI is enhanced or suppressed. Figure 4 shows a stability diagram from the Penrose criterion for Xe^+ (131AMU), Kr^+ (84 AMU), Ar^+ (40 AMU), and He^+ (4 AMU). Here helium is included to investigate the effect of a very low ion mass. Note that due to dissociation, an iodine plasma is expected to be dominated by I^+ ions [26]. Since these ions have a similar mass (127 AMU) to Xe^+, we have not explicitly included I^+ in figure 4. Figure 4 demonstrates that all propellants show similar stability behavior, but that the onset conditions can be significantly reduced for lower mass ions.

Figure 5 shows the pressure thresholds for the same propellants as in figure 4. Here we have assumed that the ions are moving at the ion sound speed, and have used approximate collision cross-sections at this speed taken from [40]. Similar to figure 4 we see that the onset conditions for instability are reduced for lighter ions, and that the unstable region is broader. This again suggests that the EDI is likely to play a role in HETs using alternative propellants.

3. Transport effects

3.1. Plasma kinetic equation

In sections 2.3 and 2.4 above we have studied conditions leading to the onset of the EDI in HETs, but we have not addressed the macroscopic consequences of this instability. In sections 3.3–3.8 below we will investigate the effect that the EDI has on the macroscopic plasma transport equations by considering the velocity moments of the relevant plasma kinetic equation. The macroscopic transport effects of kinetic instabilities have been studied previously by a number of other authors for fusion applications [41], hollow cathodes [42], magnetoplasmadynamic thrusters [43], and fundamental plasma physics [44, 45]. Here it is generally found that such instabilities lead to increased charged particle heating, as well as enhanced collisionality. In this section our aim is to investigate the macroscopic effect that the EDI has on the particle transport in HETs, and to provide simple order of magnitude estimates for determining the importance of these effects. Although the impact of the EDI on the electron momentum conservation equation has already been previously discussed in a HET context [12, 55], section 3.5 briefly highlights some of the main conclusions for completeness.

In the presence of electrostatic oscillations, the electric field and particle distribution functions can be separated into equilibrium ($\mathbf{E}$ and f_s) and fluctuating components ($\delta\mathbf{E}$ and δf_s), and the kinetic equations for the equilibrium and fluctuating components can then be written as [46, 47]

$$\frac{\partial f_s}{\partial t} + \mathbf{v}\cdot\frac{\partial f_s}{\partial \mathbf{x}} + \frac{q_s}{m_s}(\mathbf{E}+\mathbf{v}\times\mathbf{B})\cdot\frac{\partial f_s}{\partial \mathbf{v}} = \left(\frac{\partial f_s}{\partial t}\right)_{sn} - \frac{q_s}{m_s}\left\langle \delta\mathbf{E}\cdot\frac{\partial \delta f_s}{\partial \mathbf{v}}\right\rangle, \tag{18}$$

$$\frac{\partial \delta f_s}{\partial t} + \mathbf{v}\cdot\frac{\partial \delta f_s}{\partial \mathbf{x}} + \frac{q_s}{m_s}(\mathbf{E}+\mathbf{v}\times\mathbf{B})\cdot\frac{\partial \delta f_s}{\partial \mathbf{v}} = -\frac{q_s}{m_s}\delta\mathbf{E}\cdot\frac{\partial f_s}{\partial \mathbf{v}} + \frac{q_s}{m_s}\left[\left\langle \delta\mathbf{E}\cdot\frac{\partial \delta f_s}{\partial \mathbf{v}}\right\rangle - \delta\mathbf{E}\cdot\frac{\partial \delta f_s}{\partial \mathbf{v}}\right], \tag{19}$$

where $\left(\frac{\partial f_s}{\partial t}\right)_{sn}$ is a collision operator for collisions between charged particle species s and neutrals. As can be seen in equation (18), the effect of electrostatic fluctuations is to add an additional term to the right-hand side which represents the correlation between any oscillations in the electric field and the distribution function. This term effectively represents a friction force between charged particle species, and in the presence of a stable plasma consisting of electrons and ions, leads to the standard Coulomb collision formula. For completeness, and to further emphasis this point, we will rederive

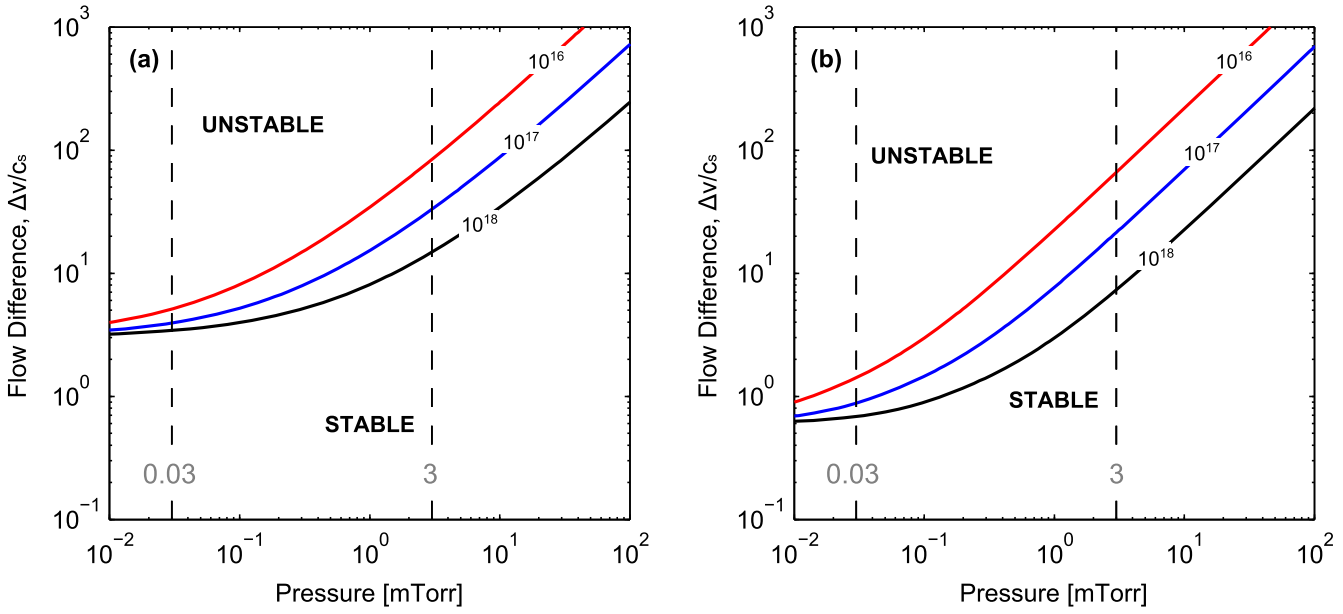

Figure 3. Electron–ion flow speed differences leading to instability as a function of neutral gas pressure for electron–ion temperature ratios of (a) $\frac{T_e}{T_i} = 20$, and (b) $\frac{T_e}{T_i} = 100$. The curves correspond to different plasma densities in units of (m^{-3}). Parameters above the curves lead to an unstable plasma. The vertical dashed lines mark pressures of 0.03 mTorr and 3 mTorr, respectively.

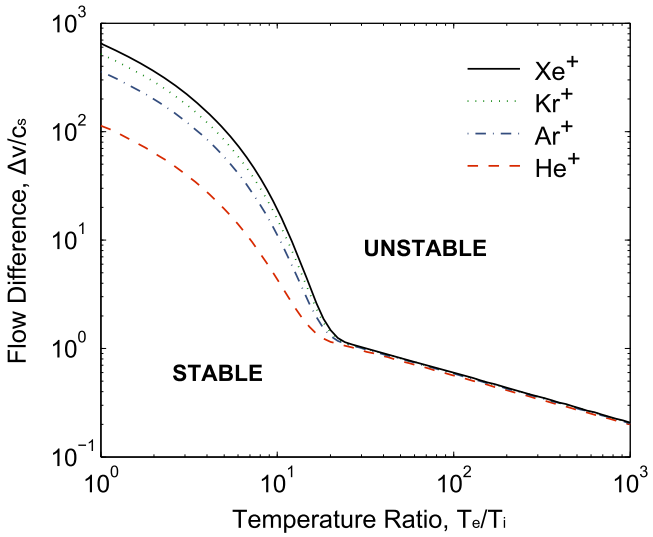

Figure 4. Electron–ion flow speed differences leading to instability as a function of electron–ion temperature ratio. The curves correspond to the different ions indicated: Xe^+, Kr^+, Ar^+, and He^+. Parameters above the curves lead to an unstable plasma.

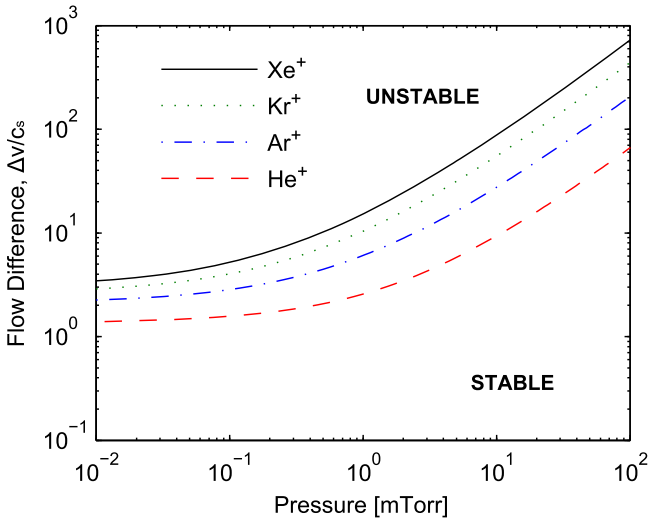

Figure 5. Electron–ion flow speed differences leading to instability as a function of neutral gas pressure. The electron–ion temperature ratio is $\frac{T_e}{T_i} = 20$, and the plasma density is 10^{17} m^{-3}. The curves correspond to the different ions indicated: Xe^+, Kr^+, Ar^+, and He^+. Parameters above the curves lead to an unstable plasma.

this formula in section 3.4 below. In an unstable plasma however, this standard Coulomb collision formula no longer applies and any instabilities can effectively enhance the electron–ion collisionality by orders of magnitude, as was recently demonstrated in a HET context in [12], and as we again show in section 3.5. In equations (18) and (19) we have ignored the presence of any fluctuating magnetic field in order to focus on electrostatic modes that have previously been observed in PIC simulations. Some studies however have suggested that fluctuating magnetic fields produced within the plasma might also contribute to an enhanced transport [48].

3.2. Instability convection

Before considering how the EDI affects the macroscopic particle conservation equations, we briefly discuss convection of the instability. In HETs the EDI initially grows in time before eventually saturating [12, 15]. At the same time it also continuously convects away in space. This growth and convection can be studied by considering a conservation equation [49] for the instability energy density (where $W \propto |\delta \mathbf{E}|^2$),

$$\frac{\partial W}{\partial t} + \nabla \cdot (\mathbf{v}_g W) = 2\gamma W. \tag{20}$$

Here the first term on the left-hand side represents growth of the instability in time, while the second term represents convection in space. In HETs the group velocity of the EDI is dominated by the axial ion drift velocity (see equation (11)) so we can approximate, $v_g \approx v_{zi}$, and thus

$$\frac{\partial W}{\partial t} \approx 2\gamma W - \frac{\partial}{\partial z}(v_{zi} W) \approx 2\gamma W - \frac{v_{zi} W}{L_{\text{acc}}} = \frac{W}{\tau_g}(1 - \alpha). \tag{21}$$

Here $\tau_g = \frac{1}{2\gamma}$, $\tau_c = \frac{L_{\text{acc}}}{v_{zi}}$, $\alpha = \frac{\tau_g}{\tau_c} = \frac{v_{zi}}{2\gamma L_{\text{acc}}}$, and L_{acc} is a characteristic length representative of the HET acceleration region. Consider now what happens when the instability first forms. If $\alpha \ll 1$, we see that the instability has a very long time to grow before it is convected away, indicating that the instability amplitude can reach very high levels. After a few growth times however the instability will reach a nonlinear regime and will eventually saturate leading to $\frac{\partial W}{\partial t} = 0$. PIC simulations suggest that this saturation occurs because of ion-wave trapping in the azimuthal direction [14, 15]. This regime was recently treated in [12]. For $\alpha > 1$ the instability cannot grow, while for, $\alpha = 1$, wave growth is just balanced by convection so that again we have, $\frac{\partial W}{\partial t} = 0$ (the instability can still grow in space though), but are now in a quasi-linear regime. This regime has been treated previously in the context of two-stream instabilities in plasmas with multiple ion species [50].

Since the parameter α controls the instability regime (i.e. quasi-linear or nonlinear) it also to a large extent determines the instability amplitude and subsequent effects on particle transport. It is therefore interesting to consider how this value depends on typical HET parameters. We can approximate the ion drift velocity as, $v_{zi} \approx \sqrt{\frac{2qV_D}{M}}$ (where V_D is the discharge voltage), and the electron azimuthal drift velocity as, $v_{ye} = \frac{E_z}{B_x} \approx \frac{V_D}{B_x L_{\text{acc}}}$. Then using equation (9) for the maximum growth rate, and simplifying, we obtain

$$\alpha \approx \sqrt{\frac{27}{\pi}} \sqrt{\frac{T_e}{V_D}} \frac{\omega_{ce}}{\omega_{pe}}. \tag{22}$$

Interestingly, this does not depend directly on the ion mass (although the choice of V_D, T_e, and n_e, are likely to depend indirectly on the mass) or the system geometry to zeroth order. A common rule of thumb [1] for HETs is that $\frac{T_e}{V_D} \sim 0.1$, and thus equation (22) becomes

$$\alpha \sim \frac{\omega_{ce}}{\omega_{pe}}. \tag{23}$$

Since $\omega_{ce} \ll \omega_{pe}$ in most HETs, we have that $\alpha \ll 1$, and thus that the EDI can be expected to grow to very large amplitudes and hence enter the nonlinear regime. In fact we see from equation (23) that only the magnetic field strength and plasma density play a role in this transition. If the magnetic field is increased too far, then $\alpha \to 1$ and the strength of the instability is expected to be significantly reduced. If this occurs, the enhanced electron–ion collisionality associated with the instability will also be strongly diminished, as well as the consequent electron cross-field transport. Depending on the operating conditions, it is possible that this could lead to intermittent/unstable thruster operation because of insufficient electron current to sustain the discharge. This cascade of events effectively occurs because the azimuthal electron drift velocity (and hence instability growth rate) is reduced with higher magnetic fields. Interestingly though, as long as the ratio $\frac{T_e}{V_D} \sim 0.1$ is maintained, increasing the discharge voltage to compensate does not seem to be an option. Fundamentally this is because increasing the discharge voltage will also increase the axial ion velocity, and hence the instability convection rate. Note that as the instability evolves in time, both the electron and ion distribution functions are expected to be modified, which would in turn change the growth rate. Thus the analysis above is only an approximate estimate, but one which nonetheless highlights the importance of instability convection and nonlinear effects.

In deriving equation (23) we have chosen the acceleration region as a convenient characteristic location, and used a representative ion velocity that most likely overestimates the true value in this region. Since the initial growth rate of the EDI is also high outside of the acceleration region, and since the ion velocity there could be lower, there may well be another location in the thruster where the growth-to-convection ratio (i.e. α) is in fact lower. This would imply that the instability has an even longer relative time to grow before being convected away, which further emphasizes our conclusion in this section.

It is interesting to note that the scaling in equation (23) has been observed numerically to play a role in HET operation. In [51] 2D PIC simulations of the z–θ directions of a HET were conducted with a scaling factor to artificially increase the permittivity of free space (so as to reduce computational requirements). As the scaling factor was reduced below a certain value, a transition was observed leading to large changes in the plasma properties and electron mobility. This transition was found to depend on the ratio, $\frac{\omega_{ce}}{\omega_{pe}}$, which is identical to our expression for α. Since changing the permittivity of free space alters ω_{pe}, this serves to again highlight the importance of the ratio of instability growth-to-convection.

3.3. Electron and ion continuity equations

The particle continuity equations are obtained by integrating equation (18) over all velocities to obtain

$$\frac{\partial n_s}{\partial t} + \frac{\partial}{\partial \mathbf{x}} \cdot (n_s \mathbf{v}_{ds}) = S_{sn}, \tag{24}$$

where n_s and $\mathbf{v}_{ds}$ are the particle density and flow/drift velocities respectively and S_{sn} is a source term accounting for collisions with neutral particles only (i.e. such as ionization). The correlation term on the right-hand side of equation (18) vanishes during integration because the distribution function must go to zero at infinite velocities. The result in equation (24) is trivial and simply demonstrates the fact that electron–ion collisions do not create or destroy particles, nor do they cause an interchange between particle species. Thus the EDI has no effect on the particle continuity equations.

3.4. Electron momentum conservation equation: stable plasma

The electron momentum conservation equation is found by multiplying equation (18) by $m\mathbf{v}$ and again integrating over all velocities

$$\frac{\partial}{\partial t}(mn_e\mathbf{v}_{de}) + \nabla\cdot(mn_e\mathbf{v}_{de}\mathbf{v}_{de}) = qn_e(\mathbf{E}+\mathbf{v}_{de}\times\mathbf{B}) - \nabla\cdot\mathbf{\Pi}_e + \mathbf{R}_{en} + \mathbf{R}_{ei} \quad (25)$$

with

$$\mathbf{R}_{ei} = q\langle\delta n_e\delta\mathbf{E}\rangle \quad (26)$$

and where $\mathbf{\Pi}_e$ is the electron pressure tensor, and $\mathbf{R}_{en}$ is the momentum loss due to electron–neutral collisions. The electron–ion friction force density, $\mathbf{R}_{ei}^{\mathrm{LB}}$, for a stable plasma (i.e. where the EDI is not present) can be determined by directly computing the correlation of density and electric field fluctuations associated with individual particles using the mean field response functions. This leads to the momentum moment of the Lenard–Balescu equation [52, 53]: $\mathbf{R}_{ei}^{\mathrm{LB}} = q\int \mathrm{d}^3v\langle\delta f_e\,\delta\mathbf{E}\rangle = \int \mathrm{d}^3v m\mathbf{v}C_{\mathrm{LB}}(f_e,f_i)$, where

$$C_{\mathrm{LB}}(f_e,f_i) = -\nabla_{\mathbf{v}}\cdot\int \mathrm{d}^3v'\mathcal{Q}_{\mathrm{LB}}^{ei}\cdot\left(\frac{f_e(\mathbf{v})}{M}\nabla_{\mathbf{v}'}f_i(\mathbf{v}') - \frac{f_i(\mathbf{v}')}{m}\nabla_{\mathbf{v}}f_e(\mathbf{v})\right) \quad (27)$$

is the Lenard–Balescu collision operator, and

$$\mathcal{Q}_{\mathrm{LB}}^{ei} = \frac{2Z^2e^4}{(4\pi\epsilon_0)^2m}\int \mathrm{d}^3k\frac{\mathbf{kk}}{k^4}\frac{\delta(\mathbf{k}\cdot\mathbf{u})}{|\hat{\varepsilon}(\mathbf{k},\mathbf{k}\cdot\mathbf{v})|^2} \approx \frac{2\pi Z^2e^4\ln\Lambda}{(4\pi\epsilon_o)^2m}\frac{u^2\mathcal{I}-\mathbf{uu}}{u^3}. \quad (28)$$

Here $e=|q|$, Z is the ion charge number, $\mathbf{u}=\mathbf{v}-\mathbf{v}'$ and the second form follows from taking the dielectric response to be the adiabatic value for a stable plasma: $\hat{\varepsilon}\approx 1+\frac{1}{k^2\lambda_{\mathrm{De}}^2}$. Assuming the electron and ion distribution functions are shifted Maxwellians, and carrying out the six velocity integrals, leads to (see appendix A of [54]):

$$\mathbf{R}_{ei}^{\mathrm{LB}} = -n_em\nu_{ei}\Delta\mathbf{v}\left[\frac{3\sqrt{\pi}}{4}\frac{\bar{v}_{ei}^3}{\Delta v^3}\psi\left(\frac{\Delta v^2}{\bar{v}_{ei}^2}\right)\right], \quad (29)$$

where

$$\nu_{ei} = \frac{16\sqrt{\pi}Z^2e^4n_i\ln\Lambda}{3(4\pi\epsilon_0)^2\,mm_{ei}\bar{v}_{ei}^3} \quad (30)$$

is the standard electron–ion collision frequency. Here, $\bar{v}_{ei}^2 = v_{Te}^2+v_{Ti}^2\approx v_{Te}^2$, $m_{ei}=\frac{mM}{m+M}\approx m$ is the reduced mass, $\ln\Lambda$ is the Coulomb logarithm, and $\psi(x)=\frac{2}{\sqrt{\pi}}\int_0^x \mathrm{d}t\sqrt{t}\exp(-t) = \mathrm{erf}(\sqrt{x}) - \frac{2}{\sqrt{\pi}}\sqrt{x}\exp(-x)$ is the Maxwell integral.

Typically, one is concerned with the slow flow limit $\frac{\Delta v}{\bar{v}_{ei}}\ll 1$, in which case the term in square brackets in equation (29) asymptotes to 1, returning the familiar expression for friction in a plasma. However, in the azimuthal direction of a HET this is not an appropriate expansion because $\frac{\Delta v}{\bar{v}_{ei}}\approx\frac{v_{ey}}{v_{Te}}\approx 1$. In this case, the term in square brackets in equation (29) is approximately 0.57 (see figure 1 of [54]). As a consequence, an estimate for the magnitude of the stable plasma electron–ion friction force density in the azimuthal direction is

$$R_{ei,y}^{\mathrm{LB}} \approx 0.57n_em\nu_{ei}v_{Te} \approx \frac{2.7n_e^2|q|^3\ln\Lambda}{(4\pi\epsilon_0)^2T_e}, \quad (31)$$

where we have used quasi-neutrality so that $n_i\approx n_e$, and assumed singly charged ions so that $Z=1$.

3.5. Electron momentum conservation equation: unstable plasma

In the case of an unstable plasma, equations (25) and (26) still equally apply, but the resulting final expression for equation (26) is different. Since we have previously treated this case in detail in [12] we quote only the final result here, which is obtained by considering the dispersion relation for the EDI, the Vlasov equation for the fluctuating electron distribution component (i.e. δf_e), and the conservation equation for the instability energy density,

$$\mathbf{R}_{ei}^{\mathrm{IE}} = -\frac{\pi q^2n_e\beta|\delta\tilde{E}|^2}{mv_{Te}^2k_y}\hat{\mathbf{j}} = -\frac{|q|}{4\sqrt{6}}\frac{1}{c_s}\,|\nabla\cdot(\mathbf{v}_{di}n_eT_e)|\,\hat{\mathbf{j}}. \quad (32)$$

Here the superscript IE refers to instability-enhanced, β is a variable representing the portion of the electron distribution function at the wave resonance (see [12] and/or section 3.6 below), and $|\delta\tilde{E}_y|$ is the amplitude of the instability electric field (assuming a single dominant sinusoidal mode at the wavevector giving the maximum growth rate). We have written two expressions in equation (32) because both will be needed in the sections below. The direction and sign of $\mathbf{R}_{ei}$ depends on the coordinate system used, as well as the direction of the electron azimuthal drift. In the coordinate system adopted here (see section 2.1) the friction force is in the azimuthal direction, and acts in the opposite direction to the electron drift, since it represents an electron–ion friction force (i.e. a momentum loss).

To demonstrate the importance of the EDI, we compare the magnitude of the instability enhanced electron–ion friction force (Equation (32) with $R_{ei}^{\mathrm{IE}}=|\mathbf{R}_{ei}^{\mathrm{IE}}|$) to the standard value for a stable plasma (equation (31)). To do this we approximate the derivative in equation (32) as $\nabla\cdot(\mathbf{v}_{di}n_eT_e)\approx\frac{\mathrm{d}}{\mathrm{d}z}(v_{iz}n_eT_e)\approx\frac{v_{iz}n_eT_e}{L_{\mathrm{acc}}}$, and $v_{iz}\approx\sqrt{\frac{2\,|\,q\,|\,V_D}{M}}$, and we then obtain

$$\frac{R_{ei}^{\mathrm{IE}}}{R_{ei,y}^{\mathrm{LB}}} \approx 8.4\sqrt{\frac{V_D}{T_e}}\frac{\epsilon_0^2T_e^2}{q^2n_eL_{\mathrm{acc}}\ln\Lambda}. \quad (33)$$

For $n_e=5\times10^{17}$ m^{-3}, $T_e=20$ eV, $L_{\mathrm{acc}}=1$ cm, and $V_D=300$ V, we obtain $\frac{R_{ei}^{\mathrm{IE}}}{R_{ei,y}^{\mathrm{LB}}}\sim 500$. Thus the instability enhanced electron–ion friction force is orders of magnitude higher than that due to standard electron–ion Coulomb collisions.

3.6. Electron energy conservation equation: stable plasma

Multiplying equation (18) by $\frac{1}{2}mv^2$ and integrating over all velocities gives the electron energy conservation equation

$$\frac{\partial}{\partial t}\left(\frac{3}{2}n_e T_e + \frac{1}{2}mn_e v_{de}^2\right) + \nabla\cdot\left[\mathbf{Q}_e + \left(\frac{5}{2}n_e T_e + \frac{1}{2}mn_e v_{de}^2\right)\mathbf{v}_{de} + \mathbf{v}_{de}\cdot\mathbf{\Pi}\right] = qn_e\mathbf{v}_{de}\mathbf{E} + P_{en} + P_{ei}, \tag{34}$$

where $\mathbf{Q}_e$ is the heat flux, P_{en} is the energy loss from electron–neutral collisions, and P_{ei} is given by

$$P_{ei} = -\frac{1}{2}q\int \mathrm{d}^3v v^2\left\langle \delta\mathbf{E}\cdot\frac{\partial\delta f_e}{\partial\mathbf{v}}\right\rangle. \tag{35}$$

Like the friction force calculated in section 3.4, P_{ei} can be computed from the appropriate correlation of fluctuating quantities associated with individual particles in the mean field response approximation. Here, this leads to the energy moment of the Lenard–Balescu equation [52, 53]: $P_{ei}^{\mathrm{LB}} = \int \mathrm{d}^3v\frac{1}{2}mv^2 C_{\mathrm{LB}}(f_e, f_i)$. Applying equations (27) and (28) and integrating by parts twice, first to remove the leading velocity-space gradient and second to remove the velocity-space gradients of f_e and f_i, leads to

$$P_{ei}^{\mathrm{LB}} = -\frac{4\pi Z^2 e^4\ln\Lambda}{m_{ei}}\int \mathrm{d}^3u\,\frac{\mathbf{u}}{u^3}\cdot\int \mathrm{d}^3v'\left(\mathbf{v}' + \frac{m_{ei}}{M}\mathbf{u}\right)f_s(\mathbf{u}+\mathbf{v}')f_{s'}(\mathbf{v}'). \tag{36}$$

Assuming the electron and ion distribution functions are shifted Maxwellians and carrying out the six velocity integrals leads to

$$P_{ei}^{\mathrm{LB}} = \left(\frac{v_{Ti}^2\mathbf{v}_{de} + v_{Te}^2\mathbf{v}_{di}}{\bar{v}_{ei}^2}\right)\cdot\mathbf{R}_{ei}^{\mathrm{LB}} - 3\frac{m_{ei}}{M}n_e\nu_{ei}(T_e - T_i)\left[\frac{\sqrt{\pi}}{2}\frac{\bar{v}_{ei}}{\Delta v}\mathrm{erf}\left(\frac{\Delta v}{\bar{v}_{ei}}\right)\right], \tag{37}$$

where $\mathbf{R}_{ei}^{\mathrm{LB}}$ is given in equation (29). Typically, one is concerned with the slow flow limit, $\frac{\Delta v}{\bar{v}_{ei}} \ll 1$, in which case the first term in equation (37) is negligible and the term in square brackets asymptotes to 1, returning the familiar expression for temperature relaxation in a plasma. Here, we are interested in the situation where $\frac{\Delta v}{\bar{v}_{ei}} \approx 1$. In this case the term in square brackets takes a values of approximately 0.75, and R_{ei} is given by equation (31). Choosing the reference frame to be the ion fluid (so $v_{di} = 0$), and the electron flow speed to be $v_{de} \approx v_{Te}$ (note that we show in section 3.8 that the ions flow at a fraction of c_s, which slightly reduces this estimate for the electron flow in the ion rest frame, but this has a negligible correction to the results of this section), and using $\bar{v}_{ei} \approx v_{Te}$, the first term in equation (37) is found to be $\frac{T_i}{T_e} \ll 1$ smaller than the second term (see section 3.9). With these, we have

$$P_{ei}^{\mathrm{LB}} \approx 4\frac{m}{M}R_{ei,y}^{\mathrm{LB}}v_{Te} \tag{38}$$

as an estimate for the electron–ion energy exchange rate. Note that this returns the familiar result from Coulomb collision theory that electron–ion energy exchange occurs more slowly than momentum exchange (i.e. friction) by a factor of the electron–ion mass ratio: $\nu_{\mathcal{E}} \sim \frac{m}{M}\nu_s$. Accounting for the large drift only influences the numerical factor in front of this expression.

3.7. Electron energy conservation equation: unstable plasma

Assuming that the instability is predominantly in the azimuthal direction, we can use integration by parts (noting that the boundary terms go to zero at infinity) with equation (35) to obtain

$$P_{ei}^{\mathrm{IE}} = q\langle\delta E_y\int \mathrm{d}^3v v_y\delta f_e\rangle = \langle\delta J_y\delta E_y\rangle. \tag{39}$$

Assuming that the instability is dominated by a single mode at the wavenumber of maximum growth rate, we can use sinusoidally varying quantities in time such that, $\delta E_y = \mathrm{Re}\{\delta\tilde{E}_y\mathrm{e}^{\mathrm{i}(k_y y-\omega_R t)}\}$, $\delta f_e = \mathrm{Re}\{\delta\tilde{f}_e\mathrm{e}^{\mathrm{i}(k_y y-\omega_R t)}\}$, and hence $P_{ei} = \langle\delta J_y\delta E_y\rangle = \frac{1}{2}\mathrm{Re}\{\delta\tilde{J}_y\delta\tilde{E}_y^*\}$. Using these expressions in equation (19) [12] and (39) we get

$$\delta\tilde{f}_e = \frac{|q|\delta\tilde{E}_y}{m}\frac{\mathrm{i}}{\omega - k_y v_y}\frac{\partial f_e}{\partial v_y}. \tag{40}$$

Thus

$$P_{ei}^{\mathrm{IE}} = -\mathrm{Re}\left\{\frac{q^2|\delta\tilde{E}_y|^2}{2m}\int \mathrm{d}^3v\frac{\mathrm{i}v_y}{\omega - k_y v_y}\frac{\partial f_e}{\partial v_y}\right\}. \tag{41}$$

Because the EDI is in the nonlinear regime, the equilibrium distribution function is unlikely to be Maxwellian. In [12] we accounted for this by using a generalized distribution given by

$$f_e = \frac{n_e}{v_{Te}^3\int \mathrm{d}^3u' g(\mathbf{u}')}g\left(\frac{\mathbf{v} - \mathbf{v}_{de}}{v_{Te}}\right), \tag{42}$$

where g is some function. Defining $\mathbf{u} = \frac{\mathbf{v}-\mathbf{v}_{de}}{v_{Te}}$, using equation (42), and simplifying, equation (41) becomes

$$P_{ei}^{\mathrm{IE}} = -\mathrm{Re}\left\{\frac{q^2 n_e|\delta\tilde{E}_y|^2}{2mv_{Te}k_y}\int_{-\infty}^{\infty}\mathrm{d}u_\parallel\frac{\mathrm{i}(u_\parallel+\eta)}{\zeta - u_\parallel}\frac{\mathrm{d}G}{\mathrm{d}u_\parallel}\right\}. \tag{43}$$

Here $G = \frac{\int \mathrm{d}^2u g(\mathbf{u}_\perp, u_\parallel)}{\int \mathrm{d}^3u' g(\mathbf{u}')}$ with $u_\parallel$ parallel to k_y and $\mathbf{u}_\perp$ perpendicular to k_y, $\eta = \frac{v_{de}}{v_{Te}}$, and $\zeta = \frac{\omega - k_y v_{de}}{k_y v_{Te}}$. Applying the Plemelj relation to the integral in equation (43) gives

$$P_{ei}^{\mathrm{IE}} = -\mathrm{Re}\left\{\frac{q^2 n_e|\delta\tilde{E}_y|^2}{2mv_{Te}k_y}\left[\mathrm{i}P\int_{-\infty}^{\infty}\mathrm{d}u_\parallel\frac{u_\parallel+\eta}{\zeta - u_\parallel}\frac{\mathrm{d}G}{\mathrm{d}u_\parallel} + \pi(\zeta+\eta)\frac{\mathrm{d}G}{\mathrm{d}u_\parallel}\bigg|_\zeta\right]\right\}, \tag{44}$$

where P represents the principal value of the integral. Taking

the real part yields

$$P_{ei}^{\mathrm{IE}} = -\frac{\pi q^2 n_e |\delta\tilde{E}_y|^2 (\zeta+\eta)}{2mv_{Te}k_y}\frac{\mathrm{d}G}{\mathrm{d}u_\parallel}\bigg|_\zeta = -\frac{\pi q^2 n_e |\delta E_y|^2 (\zeta+\eta)\beta}{mv_{Te}k_y} \quad (45)$$

where we have introduced the definition (see also [12]), $\beta = \frac{1}{2}\frac{\mathrm{d}G}{\mathrm{d}u_\parallel}\Big|_\zeta$. Substituting the magnitude of the first expression in equation (32) into (45) we have

$$P_{ei}^{\mathrm{IE}} = -R_{ei}^{\mathrm{IE}} v_{Te}(\zeta+\eta). \quad (46)$$

Here $R_{ei}^{\mathrm{IE}} = |\mathbf{R}_{ei}^{\mathrm{IE}}| \geqslant 0$. Now $\zeta = \frac{\omega - k_y v_{de}}{k_y v_{Te}} = \frac{\omega}{k_y v_{Te}} - \frac{v_{de}}{v_{Te}} = \frac{\omega}{k_y v_{Te}} - \eta \approx \frac{\omega_R}{k_y v_{Te}} - \eta$. Thus equation (46) becomes

$$P_{ei}^{\mathrm{IE}} = -R_{ei}^{\mathrm{IE}}\frac{\omega_R}{k_y} = -R_{ei}^{\mathrm{IE}} v_{\mathrm{phase}}. \quad (47)$$

Thus we have the satisfying result that the power deposition is given by the enhanced friction force multiplied by the instability phase velocity. In addition this power deposition is negative indicating that the instability takes energy from the electrons, which intuitively makes sense since the electrons lose momentum in the azimuthal direction.

We can ask how the magnitude of this new power deposition term compares with the power absorption due to the equilibrium electric field: $P_{\mathrm{abs}} = qn_e\mathbf{v}_{de}\mathbf{E}$. Since the electric field is largest in the axial direction, this power deposition term simplifies to $P_{\mathrm{abs}} \approx qn_e v_{ez}E_z$. From [12] we showed that the enhanced electron–ion friction force gives rise to an increased electron mobility that can approximately be written as

$$\mu_{\mathrm{eff}} = \frac{v_{ez}}{E_z} = \frac{\frac{|q|}{m\nu_m}}{1+\frac{\omega_{ce}^2}{\nu_m^2}}\left[1+\frac{\omega_{ce}}{\nu_m}\frac{R_{ei}^{\mathrm{IE}}}{|q|n_e E_z}\right]. \quad (48)$$

If we assume that the electron–neutral collision frequency is negligible, this reduces to

$$\mu_{\mathrm{eff}} \approx \frac{R_{ei}^{\mathrm{IE}}}{|q|n_e E_z B_x}. \quad (49)$$

Thus

$$P_{\mathrm{abs}} \approx R_{ei}^{\mathrm{IE}}\frac{E_z}{B_x} \approx R_{ei}^{\mathrm{IE}} v_{ye}. \quad (50)$$

Therefore, as a result of the instability the axial electron power deposition is enhanced and is given by the enhanced friction force multiplied by the azimuthal electron drift velocity. But

$$\left|\frac{P_{ei}^{\mathrm{IE}}}{P_{\mathrm{abs}}}\right| = \frac{v_{\mathrm{phase}}}{v_{ye}}. \quad (51)$$

Since v_{phase} is of the order of c_s (see section 2.1), we therefore see that $\frac{v_{\mathrm{phase}}}{v_{ye}} \ll 1$, and hence $\left|\frac{P_{ei}^{\mathrm{IE}}}{P_{\mathrm{abs}}}\right| \ll 1$. This demonstrates that the extra term in the electron energy conservation equation is expected to be negligible, and so long as the effect of the instability is included in fluid simulations via an enhanced mobility/collisionality/friction force in the electron momentum conservation equation, the effects of the instability appear to be 'fully' captured. This explains why previous fluid simulations have been able to reproduce experimental results by simply adding an anomalous electron mobility [36, 55, 56].

The above result is interesting because it shows that despite the instability being in the azimuthal direction, the main power deposition is in the axial direction. This occurs because in the azimuthal direction the electric field and perturbed electron current density are oscillating in time, so at some points in the cycle there is an energy gain, and at others there is an energy loss (overall though there is still a net loss). By contrast, because of the magnetic field, the electron motion in the azimuthal direction is coupled to the axial direction, so the enhanced scattering in the azimuthal direction leads to an enhanced drift velocity in the axial direction. This, together with the temporally constant (on instability time scales) axial electric field, means that the electron energy gain in this direction is always positive, and so can be significantly larger than that in the azimuthal direction.

Finally, we compare the power transferred between electrons and ions via the wave-mediated interaction with the standard Coulomb collision rate. Equations (38) and (47) provide

$$\left|\frac{P_{ei}^{\mathrm{IE}}}{P_{ei}^{\mathrm{LB}}}\right| \approx \frac{R_{ei}^{\mathrm{IE}} v_{\mathrm{phase}}}{4\frac{m}{M}R_{ei}^{\mathrm{LB}} v_{Te}} \sim \sqrt{\frac{M}{m}}\frac{R_{ei}^{\mathrm{IE}}}{R_{ei}^{\mathrm{LB}}}. \quad (52)$$

This shows that although the energy transferred by standard electron–ion collisions is $\frac{m}{M}$ smaller than the momentum transferred, energy transferred via interaction with the waves is not reduced by this scaling. However, the relevant wave speed is $v_{\mathrm{phase}} \approx \sqrt{\frac{m}{M}}v_{Te}$, compared to v_{Te}, so the overall mass scaling of the ratio of the power exchanged from each mechanism is $\sqrt{\frac{M}{m}}$. Equation (33) showed that $\frac{R_{ei}^{\mathrm{IE}}}{R_{ei}^{\mathrm{LB}}} \sim 500$, so $\frac{P_{ei}^{\mathrm{IE}}}{P_{ei}^{\mathrm{LB}}} \sim 2.5\times 10^5$. Since P_{ei}^{IE} is already small compared to the power absorbed by the equilibrium electric field, this shows that power exchanged between electrons and ions by standard Coulomb collisions is truly negligible.

3.8. Ion momentum conservation equation

Because the EDI leads to an enhanced electron–ion friction force, by momentum conservation this should also lead to an enhanced ion–electron friction force which is equal in magnitude but opposite in direction (i.e. $\mathbf{R}_{ie} = -\mathbf{R}_{ei}$). The ion momentum conservation equation is

$$\frac{\partial}{\partial t}(Mn_i\mathbf{v}_{di}) + \nabla\cdot(Mn_i\mathbf{v}_{di}\mathbf{v}_{di}) = qn_i(\mathbf{E}+\mathbf{v}_{di}\times\mathbf{B}) - \nabla\cdot\boldsymbol{\Pi}_i - M\nu_m n_i\mathbf{v}_{di} + \mathbf{R}_{in} + \mathbf{R}_{ie}, \quad (53)$$

where $\mathbf{R}_{in}$ is the momentum loss due to ion–neutral collisions. In order to get a simple idea of the effect of the enhanced ion–electron collisions, we ignore time variations in equation (53), as well as ion–neutral collisions, and assume unmagnetized

ions with an isotropic pressure tensor. Since the instability is mainly in the azimuthal direction, equation (53) becomes

$$\frac{\partial}{\partial x}(Mn_i v_{xi} v_{yi}) + \frac{\partial}{\partial y}(Mn_i v_{yi}^2) + \frac{\partial}{\partial z}(Mn_i v_{yi} v_{zi}) = qn_i E_y - \frac{\partial p_i}{\partial y} - \mathbf{R}_{ei}^{\mathrm{IE}} \cdot \hat{\mathbf{j}}. \tag{54}$$

Here we have also substituted, $\mathbf{R}_{ie}^{\mathrm{IE}} = -\mathbf{R}_{ei}^{\mathrm{IE}}$. If there are no significant large scale spatial gradients in the radial and azimuthal direction, equation (54) can be simplified to give

$$\frac{\mathrm{d}}{\mathrm{d}z}(Mn_i v_{yi} v_{zi}) = -\mathbf{R}_{ei}^{\mathrm{IE}} \cdot \hat{\mathbf{j}}. \tag{55}$$

Substituting the second expression for the electron–ion friction force in equation (26), while using quasi-neutrality so that $n_e \approx n_i$ and using $\mathbf{v}_{di} \approx v_{zi}\hat{\mathbf{k}}$ we obtain

$$\frac{\mathrm{d}}{\mathrm{d}z}(Mn_i v_{yi} v_{zi}) = \frac{|q|}{4\sqrt{6}} \frac{1}{c_s} \left| \frac{\mathrm{d}}{\mathrm{d}z}(v_{zi} n_i T_e) \right|. \tag{56}$$

Now along the length of the thruster the ion flux towards the exit increases from zero, and thus we can approximate the derivatives as: $\frac{\mathrm{d}}{\mathrm{d}z}(n_i v_{zi} v_{yi}) \approx \frac{n_i v_{zi} v_{yi}}{L_{\mathrm{acc}}}$, and $\frac{\mathrm{d}}{\mathrm{d}z}(n_i v_{zi} T_e) \approx \frac{n_i v_{zi} T_e}{L_{\mathrm{acc}}}$. Thus we can solve for the azimuthal ion velocity from equation (56) to obtain

$$v_{yi} \approx \frac{c_s}{4\sqrt{6}}. \tag{57}$$

As a result of the instability, ions undergo a rotation in the azimuthal direction with a velocity about ten times smaller than the ion acoustic speed. Since the electron–ion friction force acts to oppose the electron azimuthal drift, and since the ion–electron friction force is opposite to the electron–ion friction force, the ions drift in the same direction as the electrons. For a typical electron temperature of, $T_e = 20$ eV, xenon ions would rotate with a velocity of about 400 m s^{-1}. In [57] ion rotation has indeed been measured in a HET. The magnitude of this ion rotation was found to be between about 200 and 600 m s^{-1}, which is consistent with what is predicted here, and which is much higher than can be explained due to any residual magnetic field effects. Thus the present instability theory offers a possible reason for this 'anomalous' ion rotation.

3.9. Ion energy conservation equation

Although we saw above that the enhanced friction force does not produce any significant additional electron power deposition, this occurred in large part because the electrons are magnetized and so the azimuthal and axial directions are coupled. For the ions which are unmagnetized, this is no longer the case and so we can ask whether the instability leads to ion heating. The ion energy conservation equation is

$$\frac{\partial}{\partial t}\left(\frac{3}{2}n_i T_i + \frac{1}{2}m_i n_i v_{di}^2\right) + \nabla \cdot \left[\mathbf{q}_i + \left(\frac{5}{2}n_i T_i + \frac{1}{2}m_i n_i v_{di}^2\right)\mathbf{v}_{di} + \mathbf{v}_{di} \cdot \mathbf{\Pi}\right] = qn_i \mathbf{v}_{di}\mathbf{E} + P_{ie}. \tag{58}$$

If we use a similar analysis to that in section 3.6 for the enhanced electron power deposition term P_{ei}^{IE}, we will obtain

$$P_{ie}^{\mathrm{IE}} = -P_{ei}^{\mathrm{IE}} = R_{ei}^{\mathrm{IE}} v_{\mathrm{phase}}. \tag{59}$$

This result logically makes sense, because the friction force term previously calculated in [12] was derived for a saturated instability indicating that the wave energy density no longer increases. Thus any energy loss by electrons due to the instability must equal the energy gain by ions. To get an approximate idea of the effect of this energy gain we simplify equation (58) by ignoring any time variation, neutral collisional-energy losses, large scale gradients in the radial and azimuthal directions, the ion heat flux, and the stress tensor. Thus we obtain

$$\frac{\mathrm{d}}{\mathrm{d}z}\left[\left(\frac{5}{2}|q|n_i T_i + \frac{1}{2}m_i n_i v_{di}^2\right)v_{zi}\right] = |q|n_i v_{zi} E_z + R_{ei}^{\mathrm{IE}} v_{\mathrm{phase}}. \tag{60}$$

Since the ion drift energy is mainly in the axial direction we set $v_{di}^2 \approx v_{zi}^2 \approx \frac{2\,|\,q\,|\,V_D}{M}$, and also approximate the derivative as $\frac{\mathrm{d}}{\mathrm{d}z} \approx \frac{1}{L_{\mathrm{acc}}}$. Similarly, $E_z \approx \frac{V_D}{L_{\mathrm{acc}}}$. Substituting for R_{ei}^{IE} and simplifying, we get

$$\frac{5}{2}T_i = \frac{T_e}{4\sqrt{6}} \frac{v_{\mathrm{phase}}}{c_s}. \tag{61}$$

But since $v_{\mathrm{phase}} = \frac{\omega_R}{k_y}$, we have from equations (7) and (8) that $v_{\mathrm{phase}} = \sqrt{\frac{2}{3}}c_s$. Thus equation (61) becomes

$$T_i = \frac{T_e}{30}. \tag{62}$$

Since the electron temperature in HETs is about 20–30 eV, we see that the instability leads to ion heating with a temperature of almost 1 eV. We note that the above is just an approximate estimate of the heating effect due to the instability itself. Ion heating in the axial direction is already well known to occur because of the broad overlap between the ionization and acceleration zones [57].

4. Wall erosion

Life-time tests of a number of HETs have shown the appearance of periodic erosion patterns on both the inner and outer ceramic channel walls (see for example [27]). These periodic patterns have a wavelength of about 1 mm as well as a very slight azimuthal inclination, but the reason for their presence remains unknown. It is interesting to note that the wavelength of the EDI studied here is also of the order of 1 mm. Furthermore, at saturation the EDI is characterized by oscillations in the plasma density of about 20%–30%, as well as the appearance of a population of very high energy ions which become trapped by the electrostatic wave [9, 12, 14–16]; factors that could both conceivably lead to an enhanced erosion rate on the channel walls.

Although the EDI is predominately in the azimuthal direction, it undergoes convection in the axial direction because of the large ion drift due to acceleration by the

applied discharge voltage (see sections 2.2 and 3.2). For an ion with a velocity of, $v_{zi} \approx \sqrt{\frac{2\,|\,q\,|\,V_D}{M}}$, and an acceleration length inside the thruster of $L_{\mathrm{acc}} \approx 1$ cm, the time taken for the instability to convect out of the thruster is, $\tau_z \sim \frac{L_{\mathrm{acc}}}{v_{zi}}$. Because the speed of the instability in the azimuthal direction is about c_s (see equation (10)), in a time τ_z it will have propagated a distance, $L_y = \tau_z c_s$. For an electron temperature of 20 eV and a discharge voltage of 300 V, this gives a distance of only 1.8 mm (and hence an azimuthal inclination of about 10°). Thus the instability only travels a very short distance in the azimuthal direction before leaving the thruster, and would give the appearance of a standing wave on these time scales (consistent with the erosion patterns observed experimentally). However it is unclear yet what determines the initial phase of the instability. If the phase is determined by the thruster operating conditions/geometry, then the apparent standing wave pattern would persist over longer time scales and lead to a definite time-averaged structure. But if the phase is random, then successive waves would be expected to cancel any coherent structure so that the time-averaged erosion would be uniform. Furthermore, in our discussion above we have assumed a single mode. If multiple non-coherent modes are present then an erosion pattern would only be expected if one of the modes is dominant (with the largest amplitude occurring at the wavenumber giving the maximum growth rate for example). Although a dominant mode has been observed in PIC simulations [9, 14–17], it is not clear yet if such a mode leads to a coherent time-averaged structure. Further work is needed to clarify these issues.

5. Discussion and conclusions

5.1. Instability onset

In section 2 we have studied in detail the onset conditions leading to the formation of the EDI in HETs. The large azimuthal electron drift velocity provides the driving force for the instability which develops essentially throughout the thruster and near-plume regions. Furthermore, ion–neutral collisions are too infrequent to damp the instability, which suggests that the EDI is expected to be present in most HETs. Since the use of lighter ions reduces the required onset conditions for this instability, alternative propellants are unlikely to change this conclusion. In performing these stability analyses we have made use of the modified ion acoustic dispersion relation (equation (2)) instead of the full discrete dispersion relation (equation (1)), which is justified based on previous theoretical/numerical studies [12, 22]. Even if conditions are encountered where this is no longer strictly true, the maximum growth rate for the full dispersion relation always appears to be higher than that for the ion acoustic relation [12, 22], hence suggesting that the full dispersion relation will be unstable if the ion acoustic dispersion relation is. Although we have not directly considered secondary electron emission in our present analysis, 2D PIC simulations [16] have shown that such emission does not appear to significantly damp the EDI.

5.2. Instability convection

By considering the balance between instability growth and convection in section 3, we have identified an additional non-dimensionalized scaling parameter for HETs, $\alpha \sim \frac{\omega_{ce}}{\omega_{pe}}$. As $\alpha \to 1$, either because of an increased magnetic field or a decreased electron density, the effect of the instability on the macroscopic plasma transport is reduced. If the magnetic field is increased too far, the instability becomes too weak and the associated electron–ion friction can no longer enhance the electron cross-field transport. Since α is a function of both the electron density, and the permittivity of free space, the introduction of scaling factors in PIC simulations (in order to reduce computational times) will alter the instability evolution.

5.3. Plasma transport

In section 3 we investigated the effect of the EDI on the macroscopic plasma transport. In addition to an electron–ion friction force enhancing the electron cross-field mobility, the instability also leads to an ion rotation in the azimuthal direction that is in good agreement with that seen experimentally. Because of the magnetic field, the additional electron power deposition by the instability in the azimuthal direction is insignificant compared with that in the axial direction. From this we deduce that the anomalous electron energy loses used in the hybrid simulations in [4, 29, 30] must occur due to a different physical reason, and is most likely associated with electron energy losses and secondary electron emission at the radial thruster walls. For the ions which are unmagnetized, the power deposition by the instability can be important, and we predict that this can lead to ion heating. We highlight though that the effects of the instability on the ion transport (both ion rotation and heating) have been deduced in a very simple way and serve only as estimates. For example, although an anomalous ion rotation was experimentally measured in [57], the location of the hollow cathode was found to affect some of the results, thus possibly indicating a residual radial electric field effect. Furthermore, large scale gradients in the azimuthal direction, such as due to rotating spokes, could also very likely lead to an ion rotation.

5.4. Landau damping

Recent work [58] has suggested that an apparent discrepancy exists when considering the EDI as the cause of the anomalous electron transport in HETs. Since the azimuthal electron drift velocity (and hence instability growth rate) is largest in the acceleration region, one might also expect a very high anomalous scattering rate in this region. However, experimental measurements suggest that it is in fact the lowest in this region. Since relatively high ion temperatures [57, 59] (of a few eV) have been measured in HETs, [58] has made the interesting proposal that ion Landau damping from the main

ion beam reduces the instability growth and scattering, and that it is instead an instability associated with the presence of a second, lower energy, ion population that is responsible. Since this second population is mainly important outside of the acceleration region, anomalous scattering is small inside the thruster and largest downstream.

It is interesting to note though that the enhanced electron scattering found in section 3.5 (and discussed in more detail in [12]) already offers a second possible explanation for the above mentioned discrepancy. By considering the nonlinear effect of the instability on the electron distribution function [12] (which is significantly different from the Maxwellian used in [58]), the electron scattering in the acceleration region is naturally found to be low. This can be seen directly from equation (32). In the acceleration region the ion flux $n_i v_{zi}$ ($n_e \approx n_i$) begins to saturate as most of the propellant is ionized, while the electron temperature reaches a maximum. Thus the derivative $\frac{\mathrm{d}}{\mathrm{d}z}(v_{zi} n_i T_e)$ is low in this region, and hence so too is the electron scattering force (i.e. R_{ie}^{IE}). Physically, in this region of the discharge, although the instability amplitude is high, the electron density oscillations are almost completely out-of-phase with the electric field oscillations, resulting in a very low time-averaged scattering force [12]. Because of the typical spatial variation of the plasma properties though, the derivative $\frac{\mathrm{d}}{\mathrm{d}z}(v_{zi} n_i T_e)$ is not expected to be low/zero downstream of the thruster, and so as long as the instability is able to grow to large amplitudes (which would occur if $\alpha \ll 1$), enhanced electron transport should occur in this downstream region.

Although it is still true that high ion temperatures have been measured in HETs, these measurements are of the axial temperature. Since the instability is predominantly in the azimuthal direction, it is the azimuthal ion temperature which would be expected to determine the Landau damping rate. Both the present work, and that in [58], have however assumed isotropic ion distributions. Further work is needed to clarify the role of anisotropy in the ion distribution.

Acknowledgments

TL acknowledges financial support from a CNES post-doctoral research award. The work of SDB was supported by US Department of Energy Grant No. DE-SC0016473.

References

[1] Goebel D M and Katz I 2008 *Fundamentals of Electric Propulsion: Ion and Hall Thrusters* (New Jersey: Wiley)
[2] Zhurin V V, Kaufman H R and Robinson R S 1999 *Plasma Sources Sci. Technol.* **8** R1
[3] Morozov A I and Savelyev V V 2000 *Reviews of Plasma Physics* ed B B Kadomtsev and V D Shafranov (New York: Springer)
[4] Boeuf J P and Garrigues L 1998 *J. Appl. Phys.* **84** 3541
[5] McDonald M S 2012 Electron transport in Hall thrusters *PhD Thesis* University of Michigan
[6] Ellison C L, Raitses Y and Fisch N J 2012 *Phys. Plasmas* **19** 013503
[7] Barral S, Makowski K, Peradzyński Z and Dudeck M 2005 *Phys. Plasmas* **12** 073504
[8] Tsikata S, Cavalier J, Héron A, Honoré C, Lemoine N, Grésillon D and Coulette D 2014 *Phys. Plasmas* **21** 072116
[9] Adam J C, Héron A and Laval G 2004 *Phys. Plasmas* **11** 295
[10] Ducrocq A, Adam J C, Héron A and Laval G 2006 *Phys. Plasmas* **13** 102111
[11] Choueiri E Y 2001 *Phys. Plasmas* **8** 1411
[12] Lafleur T, Baalrud S D and Chabert P 2016 *Phys. Plasmas* **23** 053503
[13] Tsikata S, Lemoine N, Pisarev V and Grésillon D M 2009 *Phys. Plasmas* **16** 033506
[14] Boeuf J P 2014 *Front. Phys.* **2** 74
[15] Lafleur T, Baalrud S D and Chabert P 2016 *Phys. Plasmas* **23** 053502
[16] Héron A and Adam J C 2013 *Phys. Plasmas* **20** 082313
[17] Coche P and Garrigues L 2014 *Phys. Plasmas* **21** 023503
[18] Taccogna F, Minelli P, Capitelli M and Longo S 2012 *AIP Conf. Proc.* **1501** 1390
[19] Taccogna F and Minelli P 2015 *Joint Conf. of 30th Int. Symp. on Space Technology and Science 34th Int. Electric Propulsion Conf. and 6th Nano-satellite Symp.* (Hyogo-Kobe, Japan: The Electric Rocket Propulsion Society) IEPC-2015-418
[20] Frias W, Smolyakov A I, Kaganovich I D and Raitses Y 2013 *Phys. Plasmas* **20** 052108
[21] Matyash K, Schneider R, Mazouffre S, Tsikata S, Raitses Y and Diallo A 2013 *33rd Int. Electric Propulsion Conf.* (Washington, DC: The Electric Rocket Propulsion Society) IEPC-2013-307
[22] Cavalier J, Lemoine N, Bonhomme G, Tsikata S, Honoré C and Grésillon D 2013 *Phys. Plasmas* **20** 082107
[23] Lazurenko A, Coduti G, Mazouffre S and Bonhomme G 2008 *Phys. Plasmas* **15** 034502
[24] Linnell J A and Gallimore A D 2006 *J. Propul. Power* **22** 1402
[25] Szabo J, Pote B, Paintal S, Robin M, Hillier A, Branam R D and Huffman R E 2012 *J. Propul. Power* **28** 848
[26] Grondein P, Lafleur T, Chabert P and Aanesland A 2016 *Phys. Plasmas* **23** 033514
[27] Dudeck M, Doveil F, Arcis N and Zurbach S 2012 *IOP Conf. Ser.: Mater. Sci. Eng.* **29** 012010
[28] de Grys K, Mathers A, Welander B and Khayms V 2008 *46th AIAA/ASME/SAE/ASEE Joint Propulsion Conf. & Exhibit* (Nashville, TN: American Institute of Aeronautics and Astronautics) AIAA-2010-6698
[29] Hagelaar G J M, Bareilles J, Garrigues L and Boeuf J P 2002 *J. Appl. Phys.* **91** 5592
[30] Bareilles J, Hagelaar G J M, Garrigues L, Boniface C, Boeuf J P and Gascon N 2004 *Phys. Plasmas* **11** 3035
[31] Adam J C *et al* 2008 *Plasma Phys. Control. Fusion* **50** 124041
[32] Garrigues L, Pérez-Luna J, Lo J, Hagelaar G J M, Boeuf J P and Mazouffre S 2009 *Appl. Phys. Lett.* **95** 141501
[33] Scharfe M K, Gascon N, Cappelli M A and Fernandez E 2006 *Phys. Plasmas* **13** 083505
[34] Hofer R R, Katz I, Mikellides I G, Goebel D M, Jameson K K, Sullivan R M and Johnson L K 2008 *44th AIAA/ASME/SAE/ASEE Joint Propulsion Conf. & Exhibit* (Hartford, CT: American Institute of Aeronautics and Astronautics) AIAA-2008-4924
[35] Mikellides I G and Katz I 2012 *Phys. Rev.* E **86** 046703
[36] Ortega A L and Mikellides I G 2016 *Phys. Plasmas* **23** 043515
[37] Fried B D and Conte S D 1961 *The Plasma Dispersion Function* (New York: Academic)
[38] Penrose O 1960 *Phys. Fluids* **3** 258

[39] Davidson R C 1972 *Methods in Nonlinear Plasma Theory* (New York: Academic)
[40] Phelps A V 2005 *Compilation of Atomic and Molecular Data* see (http://jila.colorado.edu/∼avp/collision_data/ionneutral/IONATOM.TXT)
[41] Davidson R C and Krall N A 1977 *Nucl. Fusion* **17** 1313
[42] Jorns B A, Ortega A L and Mikellides I 2016 *52nd AIAA/SAE/ASEE Joint Propulsion Conf., AIAA Propulsion and Energy Forum* (Salt Lake City, UT: American Institute of Aeronautics and Astronautics) AIAA 2016-4626
[43] Choueiri E 1999 *Phys. Plasmas* **5** 2290
[44] Lampe M, Manheimer W M, McBride J B, Orens J H, Papadopoulos K, Shanny R and Sudan R N 1972 *Phys. Fluids* **15** 662
[45] Lampe M, Manheimer W M, McBride J B, Orens J H, Shanny R and Sudan R N 1971 *Phys. Rev. Lett.* **26** 1221
[46] Baalrud S D 2010 Kinetic theory of instability-enhanced collective interactions in plasma *PhD Thesis* University of Wisconsin-Madison
[47] Baalrud S D, Callen J D and Hegna C C 2008 *Phys. Plasmas* **15** 092111
[48] Wei L, Han K, Wang Ch, Zhang Ch and Yu D 2012 *Contrib. Plasma Phys.* **52** 761
[49] Stix T H 1992 *Waves in Plasmas* (New York: Springer)
[50] Baalrud S D, Hegna C C and Callen J D 2009 *Phys. Rev. Lett.* **103** 205002
[51] Coche P 2013 Modélisation cinétique d'un propulseur à effet Hall *PhD Thesis* Universitéde Toulouse
[52] Lenard A 1960 *Ann. Phys.* **3** 390
[53] Balescu R 1960 *Phys. Fluids* **3** 52
[54] Baalrud S D and Hegna C C 2011 *Phys. Plasmas* **18** 023505
[55] Katz I, Mikellides I G, Jorns B A and Ortega A L 2015 *Joint Conf. 30th Int. Symp. on Space Technology and Science 34th Int. Electric Propulsion Conf. and 6th Nano-satellite Symp.* (Hyogo-Kobe, Japan: The Electric Rocket Propulsion Society) IEPC-2015-402
[56] Cappelli M A, Young C V, Cha E and Fernandez E 2015 *Phys. Plasmas* **22** 114505
[57] Mazouffre S 2013 *Plasma Sources Sci. Technol.* **22** 013001
[58] Katz I, Ortega A L, Jorns B A and Mikellides I G 2016 *52nd AIAA/ASME/SAE/ASEE Joint Propulsion Conf.* (Salt Lake City, UT: American Institute of Aeronautics and Astronautics) AIAA-2016-4534
[59] Huang W, Drenkow B and Gallimore A D 2009 *45th AIAA/ASME/SAE/ASEE Joint Propulsion Conf. & Exhibit* (Denver, Colorado: American Institute of Aeronautics and Astronautics) AIAA-2009-5355